Journal of Applied Science, Engineering, Technology and Management
Vol. 02, Issue 02, December 2024 pp. 33 - 36

Synthesis, Characterization, And Photocatalytic Application of Graphitic Carbon Nitride

J Jassi
Post Graduate and Research Department of Physics, Mar Athanasius College (Autonomous), Kothamangalam, Ernakulam, Kerala, 686 666, India
jassi.jayaraj@gmail.com

S Deepa
Post Graduate and Research Department of Physics, Mar Athanasius College (Autonomous), Kothamangalam, Ernakulam, Kerala, 686 666, India
sdeepa@macollege.in

Mariyam B Tharian
Post Graduate and Research Department of Physics, Mar Athanasius College (Autonomous), Kothamangalam, Ernakulam, Kerala, 686 666, India
mariyambtharian1@gmail.com

Abstract — Graphitic Carbon Nitride (g-C_3N_4) is a polymeric semiconductor with a bandgap of 2.7eV, enabling it to absorb visible light. In this paper, g-C_3N_4 was synthesized by heating urea and thiourea separately for 2 hours at 550^{0}C in a muffle furnace. The resulting products were named g-C_3N_4-U and g-C_3N_4-T, and investigated in terms of their crystal structure, morphology, and optical properties using X-Ray Diffractometer (XRD), Field Emission Scanning Electron Microscope (FESEM), UV-visible spectrophotometer, and Photoluminescence spectrometer. Brunauer-Emmett-Teller (BET) measurements were carried out to further observe the surface area, pore size, and pore volume of the as-prepared samples. The photocatalytic activity of the samples was investigated for pollution removal purposes, and its performance was examined under direct sunlight. The results showed that the urea-derived g-C_3N_4 exhibited better photocatalytic activity, with complete degradation of the target pollutant within 90 minutes.

Keywords — Graphitic Carbon Nitride, Photocatalysis, Photocatalyst, Urea, Thiourea.

I. Introduction

Carbon nitride, primarily consisting of covalent bonds, has emerged with great interest in recent years, particularly as an equivalent to carbon in various material applications. This interest is propelled by theoretical predictions suggesting that the β-C_3N_4 phase possesses hardness comparable to that of diamond, thus positioning it as a promising candidate for diverse applications [1]. Molina et al. conducted a systematic study of the structural and electronic properties of six phases of carbon-nitride. Structural analysis shows that the N atoms behave in a pure sp^2 configuration only in the beta and graphitic phases, and the graphitic phase is considered the most stable under normal conditions [2].

Graphitic Carbon Nitride (g-C_3N_4) is a polymeric metal-free semiconducting material that has gained significant scientific interest with a bandgap of 2.7 eV, suitable for absorbing visible light [3]. The absorption in the blue region of the visible spectrum pointed out that the bandgap of condensed graphitic carbon nitride is substantial enough to counteract the endothermic nature of the water–splitting reaction, which theoretically demands 1.23 eV [4]. Li et al discovered that the g-C_3N_4 catalysts, when modified with certain co-catalysts such as Ag and NiS, achieved excellent photocatalytic hydrogen generation under visible light [5].

The photocatalytic activity of g-C_3N_4 is constrained by two factors: the rapid recombination of the photo-generated charge carriers and the narrow range of excitation wavelengths that the photocatalyst can absorb [6,7]. To fulfil industrial requirements for efficiency and stability, various strategies have been investigated to augment photo-catalytic performance and durability. A study by Jiang et al. highlights the potential of sulphur-doped g-C_3N_4 as a highly effective photocatalyst for hydrogen production [8], and Song et al. says that the composite photocatalyst Ag/g-C_3N_4 emerges as a noteworthy material for purifying pollutants [9]. Studies by Ge et al. show that the metal-free g-C_3N_4 performs well in photo-oxidation of organic pollutants [10, 11].

II. Materials and Methods

To prepare graphitic carbon nitride (g-C_3N_4), urea and thiourea were procured and used without any additional treatment. The process of preparing g-C_3N_4 involves heating both urea and thiourea separately in a furnace at 550 degrees Celsius for approximately two hours. To begin, 5 grams each of urea and thiourea were weighed and placed in separate silica crucibles. Silica crucibles are commonly used in laboratories for heating chemicals at high temperatures. Aluminium foils were used to cover the crucible to reduce unwanted reactions. During this time, the urea and thiourea undergo a chain of chemical reactions, resulting in the formation of g-C_3N_4. The resultant powders derived from thiourea and urea were named g-C_3N_4-T and g-C_3N_4-U, respectively, and were analyzed by XRD, UV-Visible Spectroscopy, FESEM, Photoluminescence, and BET analysis. The g-C_3N_4 samples were evaluated for their ability to degrade methyl orange (MO) photocatalytically in an aqueous solution under visible light. For that, 0.01 g of the prepared sample was mixed with a 100 ml MO solution (10 mg/l). The solution was magnetically stirred for half an hour to achieve MO absorption onto the catalyst. At time intervals of 20 minutes, the suspension was collected and centrifuged at 3000 rpm for 5 minutes to remove the photocatalysts. The MO concentrations were investigated by recording UV-Vis spectra.

eISSN 2584-0371

Received for review: 20-08-2024
Accepted for publication: 17-10-2024
Published: 23-10-2024

III. Analyzing Techniques

Rigaku Miniflex 600 X-ray diffraction (XRD) machine with a power of 600 W and a voltage of 40 kV, which produces X-rays with a wavelength of 1.5405 angstroms, was used to analyze the microstructural properties of the prepared samples. The surface morphology of the prepared samples was studied using Field Emission Scanning Electron Microscopy (FESEM) with the Carl Zeiss Sigma HV instrument. The UV-visible absorption spectra of the samples were recorded at room temperature using a SHIMADZU 2450 UV-visible spectrophotometer.

The Photoluminescence spectra of the samples were recorded at room temperature using HORIBA Fluorescence spectrometer at an excitation wavelength of 390 nm. The specific surface area, pore size, and pore volume of the synthesized samples were determined using a surface area analyzer (Altamira Instruments TB 440A).

IV. Results and Discussion

A. *Characterization of g-C_3N_4*

Figure 1 shows the XRD profiles of the as-prepared g-C_3N_4 samples. The diffraction peaks appear at an angle of 13.05^0 and 27.65^0 and can be indexed to (100) and (002) of graphitic materials. The (100) plane corresponds to the in-plane structural packing motif of triazine units, and (002) corresponds to the interlayer stacking of aromatic units of the CN [12].

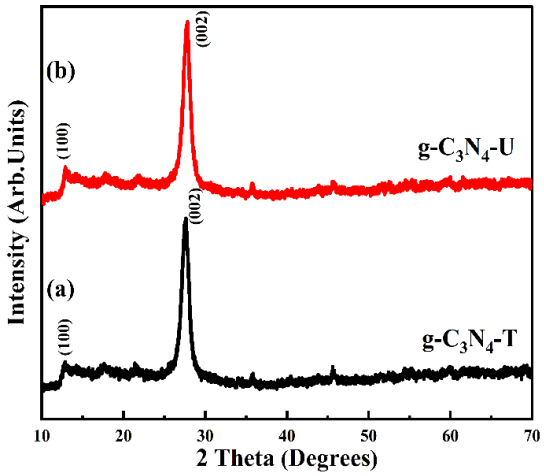

Fig.1. XRD pattern of (a) g-C_3N_4-T and (b) g-C_3N_4-U.

The morphology of g-C_3N_4 is studied by FESEM. Figure 2 shows the FESEM images of g-C_3N_4-T and g-C_3N_4-U samples. FESEM images show a flake-like structure with porous morphology. Agglomeration of nanosheets is observed in g-C_3N_4-T, whereas g-C_3N_4-U shows less agglomeration. The lamellar nanosheet like structure ensures a large effective surface area, which may be helpful in enhancing the photocatalytic activity. The nanosheet distribution is uniform.

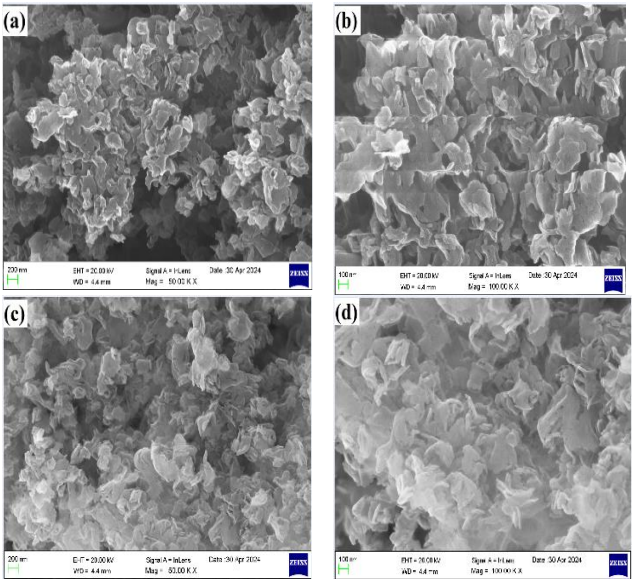

Fig. 2 FESEM images of (a), (b) g-C_3N_4 -T and (c), (d) g-C_3N_4-U at different magnifications

The absorption profile of the g-C_3N_4 derived from thiourea and urea was studied using a UV-visible spectrometer. The wavelength versus absorbance graph is shown in Figure 3. The UV-visible spectrum of g-C_3N_4 -T exhibited more absorption in the visible region than g-C_3N_4 -U. The absorption peak of g-C_3N_4 -T is around 400nm whereas, the peak redshifts to 413nm in g-C_3N_4 -U.

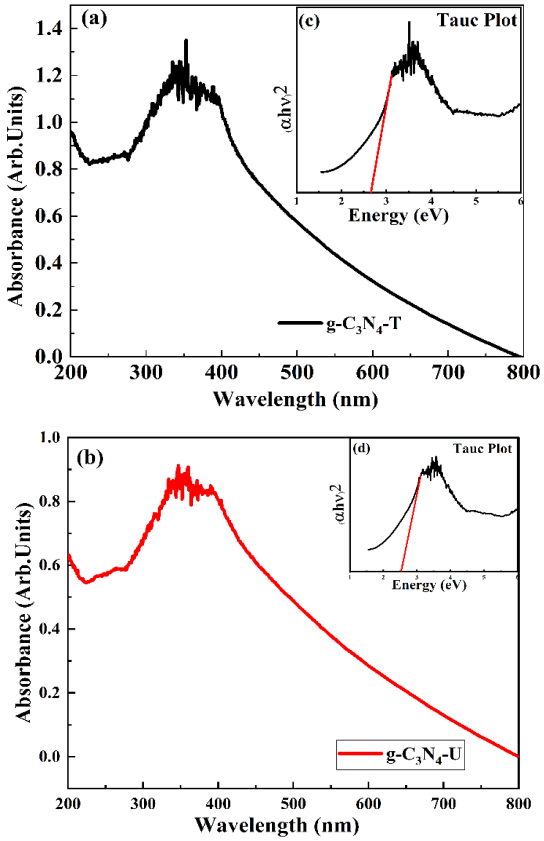

Fig.3. UV-visible absorption spectra and Tauc plots of (a, c) g-C_3N_4-T and (b, d) g-C_3N_4-U.

The change in the band structure is examined by using a Tauc plot, and the bandgap of g-C_3N_4 -T and g-C_3N_4-U are calculated as 2.62 eV and 2.52 eV, respectively. The band gap of synthesized samples depends on the type of starting materials used. This points to the possibility of tailoring the band gap by the proper selection of starting materials, which can be employed for specific applications.

The photoluminescence studies of the samples were carried out at room temperature with an excitation wavelength of 390 nm (Figure 4). Photoluminescence intensity provides insights into the recombination of charge carriers [13,14]. Both samples exhibit photoluminescence emission in the range of 400-600 nm.

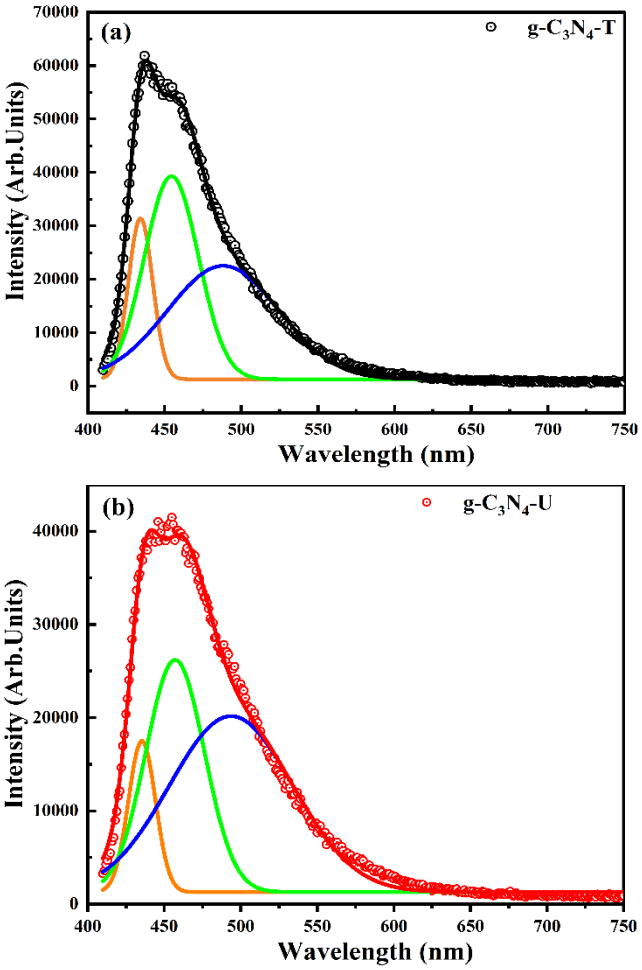

Fig.4. Photoluminescence spectra with deconvoluted peaks of (a) g-C_3N_4-T and (b) g-C_3N_4-U.

TABLE I: DECONVOLUTED PEAKS OF G-C_3N_4-T AND G-C_3N_4-U

Sample Code	g-C_3N_4-T	g-C_3N_4-U
Peak 1 (nm)	434.37	434.84
Peak 2 (nm)	454.06	457.41
Peak 3 (nm)	488.35	494.41

It is evident that the photoluminescence intensity of g-C_3N_4-T is higher compared to g-C_3N_4-U. Gaussian fitting was carried out to identify the constituent peaks. Three peaks were identified and tabulated (Table 1). Compared to g-C_3N_4 -T sample, there is a redshift in the peak position in g-C_3N_4 -U sample.

By N_2 adsorption-desorption technique, BET surface area, pore diameter, and pore volume were determined. Fig.5 shows the N_2 adsorption-desorption isotherms of the prepared samples g-C_3N_4 -T and g-C_3N_4-U.

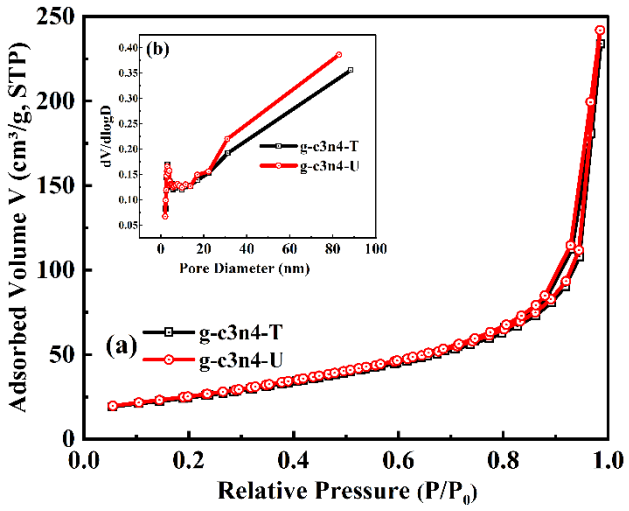

Fig.5. (a) Nitrogen adsorption-desorption isotherms and (b) corresponding pore size distribution of g-C_3N_4-T and g-C_3N_4-U.

The comparison of the surface area, pore diameter, and pore volume of the g-C_3N_4 – T and g-C_3N_4-U are presented in Table 2. g-C_3N_4-U exhibits a higher surface area than g-C_3N_4-T. The prominent hysteresis loops indicate the mesoporous nature (2-50 nm) of these g-C_3N_4-T and g-C_3N_4-U. The adsorption branch of nitrogen isotherms displays a steady increase as P/P_0 approaches unity, suggesting the formation of mesopores and small macropores [15].

TABLE II: COMPARISON OF SPECIFIC SURFACE AREA, PORE DIAMETER, AND PORE VOLUME OF THE G-C_3N_4-T AND G-C_3N_4-U

Sample code	Specific surface area ($m^2 g^{-1}$)	Pore diameter (nm)	Pore Volume ($cm^3 g^{-1}$)
g-C_3N_4-T	89.001	16.256	0.362
g-C_3N_4-U	91.894	16.285	0.374

The photocatalytic activity of the prepared samples was studied using the organic dye methyl orange under visible light [16]. The prepared photocatalyst in the MO solution was allowed in the dark for 30 minutes under continuous stirring to acquire adsorption/desorption equilibrium.

Fig. 6 (a) represents the changes in the UV-visible absorption spectra of methyl orange solution recorded at time intervals of 20 min exposure to sunlight in the presence of g-C_3N_4-U. g-C_3N_4-U showed excellent performance with 100% degradation of Methyl orange on 90 minutes of visible light exposure compared to g-C_3N_4-T (Fig. 6(b)). It can be concluded that g-C_3N_4-U synthesized from urea limits the recombination of charge carriers, resulting in excellent photocatalytic performance, as evident by photoluminescence studies.

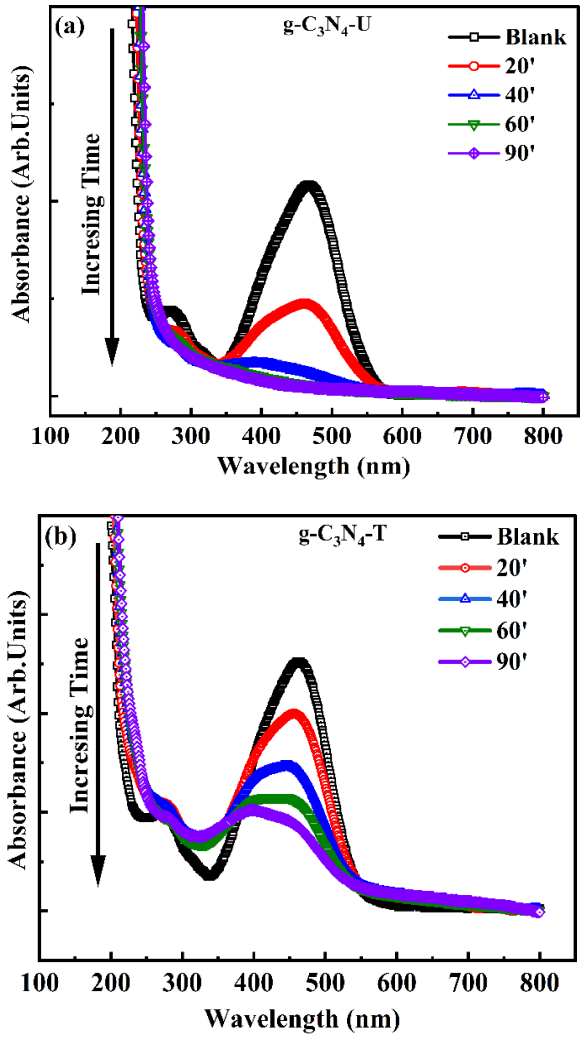

Fig. 6. Photocatalytic degradation of Methylene Orange by (a) g-C3N4-U and (b) g-C3N4-T.

V. CONCLUSIONS

This study provided an overview of both g-C_3N_4-T and g-C_3N_4-U, focusing on their fabrication, characterization, and photocatalytic application. UV-Vis spectroscopy confirmed that the bandgap of g-C_3N_4-T is 2.62 eV and that of g-C_3N_4-U is 2.52 eV. The photocatalytic efficiency of the samples was studied by photodegrading the methyl orange by exposing the samples to direct sunlight. The type of starting material has a considerable effect on the photocatalytic performance of g-C_3N_4. The study shows that g-C_3N_4-U demonstrates superior photocatalytic activity to that of g-C_3N_4-T. The present study reveals that urea-derived g-C_3N_4 is best for photocatalytic degradation of methyl orange.

ACKNOWLEDGEMENT

The authors acknowledge the Indian Science Technology and Engineering Facilities Map (I-STEM) for photoluminescence measurements. The authors also thank the MA College, Kothamangalam, for providing the research facilities.

REFERENCES

[1] Amy Y. Liu, Marvin L. Cohen, "Prediction of New Low Compressibility Solids". Science 245, pp. 841-842, (1989). DOI:10.1126/science.245.4920.841

[2] Molina, B. and Sansores, L.E., 1999. Electronic structure of six phases of C 3 N 4: a theoretical approach. Modern physics letters B, 13(06n07), pp.193-201.

[3] Wang, X., Maeda, K., Thomas, A., Takanabe, K., Xin, G., Carlsson, J.M., Domen, K. and Antonietti, M., 2009. A metal-free polymeric photocatalyst for hydrogen production from water under visible light. *Nature materials*, *8*(1), pp.76-80.

[4] Ng, C.H., Teo, S.H., Mansir, N., Islam, A., Joseph, C.G., Hayase, S. and Taufiq-Yap, Y.H., 2021. Recent advancements and opportunities of decorated graphitic carbon nitride toward solar fuel production and beyond. *Sustainable Energy & Fuels*, *5*(18), pp.4457-4511.

[5] Li, Z., Ma, Y., Hu, X., Liu, E. and Fan, J., 2019. Enhanced photocatalytic H2 production over dual-cocatalyst-modified g-C3N4 heterojunctions. *Chinese Journal of Catalysis*, *40*(3), pp.434-445.

[6] Tian, N., Huang, H., Guo, Y., He, Y. and Zhang, Y., 2014. A g-C3N4/Bi2O2CO3 composite with high visible-light-driven photocatalytic activity for rhodamine B degradation. *Applied surface science*, *322*, pp.249-254.

[7] Shao, L., Jiang, D., Xiao, P., Zhu, L., Meng, S. and Chen, M., 2016. Enhancement of g-C3N4 nanosheets photocatalysis by synergistic interaction of ZnS microsphere and RGO inducing multistep charge transfer. *Applied Catalysis B: Environmental*, *198*, pp.200-210.

[8] Jiang, J., Xiong, Z., Wang, H., Liao, G., Bai, S., Zou, J., Wu, P., Zhang, P. and Li, X., 2022. Sulfur-doped g-C3N4/g-C3N4 isotype step-scheme heterojunction for photocatalytic H2 evolution. *Journal of Materials Science & Technology*, *118*, pp.15-24.

[9] Song, Y., Qi, J., Tian, J., Gao, S. and Cui, F., 2018. Construction of Ag/g-C3N4 photocatalysts with visible-light photocatalytic activity for sulfamethoxazole degradation. *Chemical Engineering Journal*, *341*, pp.547-555.

[10] Ge, L., 2011. Synthesis and photocatalytic performance of novel metal-free g-C3N4 photocatalysts. *Materials Letters*, *65*(17-18), pp.2652-2654.

[11] Mishra, A., Mehta, A., Basu, S., Shetti, N.P., Reddy, K.R. and Aminabhavi, T.M., 2019. Graphitic carbon nitride (g–C3N4)–based metal-free photocatalysts for water splitting: a review. *Carbon*, *149*, pp.693-721.

[12] Dong, F., Zhao, Z., Xiong, T., Ni, Z., Zhang, W., Sun, Y. and Ho, W.K., 2013. In situ construction of g-C3N4/g-C3N4 metal-free heterojunction for enhanced visible-light photocatalysis. *ACS applied materials & interfaces*, *5*(21), pp.11392-11401.

[13] Li, K., Chen, M., Chen, L., Zhao, S., Xue, W., Han, Z. and Han, Y., 2023. "Synthesis of g-C3N4 derived from different precursors for photodegradation of sulfamethazine under visible light. *Processes"*, *11*(2), p.528.

[14] Hang, L.T., Lai, N.D., Phuong, N.T., Thang, D.V., Hung, N.M. and Van Minh, N., 2018." Influence of annealing temperature on physical properties and photocatalytic ability of g-C3N4 nanosheets synthesized through urea polymerization in Ar atmosphere". *Physica B: Condensed Matter*, *532*, pp.48-53.

[15] Dong, H., Guo, X., Yang, C. and Ouyang, Z., 2018. Synthesis of g-C3N4 by different precursors under burning explosion effect and its photocatalytic degradation for tylosin. *Applied Catalysis B: Environmental*, *230*, pp.65-76.

[16] Ge, L., 2011. Synthesis and photocatalytic performance of novel metal-free g-C3N4 photocatalysts. *Materials Letters*, *65*(17-18), pp.2652-2654.